Photocatalytic ozonation of metronidazole by synthesized zinc oxide nanoparticles immobilized on montmorillonite

CrossMark

Alireza Khataee [a,b,*], Murat Kıranşan [c], Semra Karaca [c,**], Mohsen Sheydaei [d]

[a] Research Laboratory of Advanced Water and Wastewater Treatment Processes, Department of Applied Chemistry, Faculty of Chemistry, University of Tabriz, 51666-14766 Tabriz, Iran
[b] Department of Materials Science and Nanotechnology Engineering, Near East University, 99138 Nicosia, North Cyprus, Mersin 10, Turkey
[c] Department of Chemistry, Faculty of Science, Atatürk University, 25240 Erzurum, Turkey
[d] Faculty of Chemistry, Kharazmi University, 15719-14911 Tehran, Iran

ARTICLE INFO

ABSTRACT

Released antibiotics in the aquatic environment have undesirable biological and ecotoxicological effects. In this work, photocatalytic ozonation process was used for removal of metronidazole (MET) as commonly used antibiotic from aqueous media. ZnO nanoparticles as an effective photocatalyst were immobilized on the surface of montmorillonite (MMT). The ZnO/MMT catalyst was characterized by X-ray diffraction (XRD), N_2 adsorption/desorption, Fourier transform infrared (FT-IR), scanning electron microscope (SEM), and high resolution transmission electron microscope (HR-TEM). The ZnO/MMT activity was examined in the degradation of metronidazole under ozone bubbling and UV-A irradiation through photocatalytic ozonation process. The main influence factors on the photocatalytic ozonation activity such as ZnO/MMT dosage, pH, metronidazole initial concentration and ozone flow rate were studied. The results indicated that the MET removal efficiency was increased with increasing all the investigated factors except initial MMT concentration. The effect of organic and inorganic radical scavengers on the photocatalytic ozonation of MET was studied. Finally, several by products were identified by GC–MS analysis, which allowed to depict a possible mechanism for the MET degradation.

© 2017 Taiwan Institute of Chemical Engineers. Published by Elsevier B.V. All rights reserved.

1. Introduction

In the past decade production and consumption of pharmaceutical compounds have been increased across the developed world. Antibiotics are a large family of pharmaceutical compounds consumed in human and veterinary for therapeutic purposes [1]. Antibiotics are released in the aquatic environment mostly from human excretion, veterinary clinics and runoff from agricultural applications [2]. This kind of pharmaceutical compounds have antibacterial nature. Therefore, the presence of the antibiotics in water resources even at very low concentrations leads to enhancement of the bacterial resistance against antibiotics [3]. Accordingly, their presence in the aquatic environment is undesirable.

Due to antibacterial nature of antibiotics, oxidation potential of conventional biological treatments is not enough to oxidize and degrade these pharmaceutical products [2]. For example, metronidazole as one of the most frequently used compounds that encompass most gram-positive and gram-negative anaerobic bacteria and protozoans. Furthermore, this antibiotic is very stable even under UV light irradiation [4]. Accordingly, various treatment techniques and processes have been developed and used to remove these compounds from polluted sources. Among these techniques, advanced oxidation processes (AOPs) have been recognized as promising approach for complementary degradation of organic pollutants from contaminated water resources [5]. AOPs are based on the generation of highly reactive and nonselective radicals especially hydroxyl radicals, which are effective oxidant toward organic compounds.
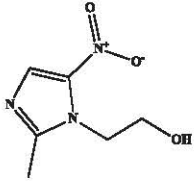
In recent years attention has been focused on heterogeneous photocatalysis as one of the most promising AOPs. In this process, semiconductors with high photocatalytic activity such as TiO_2 and ZnO particles are irradiated by UV or visible light as energy source. This energy leads to the excitation of electrons (e^-) from valence band of semiconductor into the conduction band and development of holes (h^+) in the valence band. Reaction of h^+ with H_2O or OH^- leads to reactive radicals development [6].

* Corresponding author at: Research Laboratory of Advanced Water and Wastewater Treatment Processes, Department of Applied Chemistry, Faculty of Chemistry, University of Tabriz, 51666-14766 Tabriz, Iran.
** Corresponding author.
E-mail addresses: ar_khataee@yahoo.com, a_khataee@tabrizu.ac.ir (A. Khataee), semra_karaca@yahoo.com (S. Karaca).

Table 1
Characteristics of the metronidazole.

Name	Chemical structure	Molecular formula	M_w (g/mol)	λ_{max} (nm)	Class
Metronidazole		$C_6H_9N_3O_3$	171.15	317	Antibiotic

Although different works have been reported to date for the use of ZnO photocatalysis for photodegradation of organic pollutants, some limitations have been recognized for this including: separation of semiconductor powders from batch slurry photoreactor and higher tendency of photo-generated e^-/h+ to recombine rather than contribution in the formation of reactive radicals which imposes low efficiency of photocatalytic degradation [7].

Application of ozone assisted photocatalytic degradation is one of the effective methods to overcome the mentioned limitations. O_3 molecules as a strong inorganic oxidative species can trap the photo-generated electrons and increase h+ contribution in the formation of reactive radicals. Furthermore, O_3/UV process is one of the successful AOPs for degradation of various organic pollutants in water. In recent decades, investigation of photocatalytic ozonation process ability in degradation of organic pollutants has been made in several works for instance, photocatalytic ozonation of oxalic acid by g-C_3N_4/graphene composites by Yin et al., [8], phenazopyridine by TiO_2 nanoparticles thin film by Fathinia et al., [9], urban wastewater and surface water using immobilized TiO_2 by Moreira et al., [10] and amoxicillin and diclofenac using TiO_2 by Moreira et al., [11].

The scope of this study was to immobilize ZnO nanoparticles on the surface of montmorillonite (MMT) and evaluate the application of ozone assisted photocatalytic degradation to overcome the ZnO photocatalysis limitations to use for photocatalytic degradation of the MET as organic pollutant.

2. Materials and methods

2.1. Materials and reagents

Montmorillonite K10 was purchased from Sigma-Aldrich Co., USA. This solid consists of SiO_2, Al_2O_3, Fe_2O_3, MgO, CaO, Na_2O and K_2O with wt. % of 66.9, 13.8, 2.75, 1.58, 0.29, 0.15 and 1.65, respectively. Cation exchange capacity (CEC) of the MMT was 120 meq/ 100 g. Metronidazole ($C_6H_9N_3O_3$) was purchased (Sigma-Aldrich, St. Louis, MO, USA) and dissolved in distilled water. Table 1 shows the structure and properties of MET in this study. All other utilized reagents were of analytical grade (Sigma-Aldrich, St. Louis, MO, USA) and were used as received without further purification. Distilled water was used throughout the experiments.

2.2. Preparation of ZnO/MMT nanocomposite

The ZnO/MMT nanocomposite was prepared using the following method including: Step one—development of MMT suspension by dispersion of 1 g of MMT in 100 mL distilled water. Step two—dropwise addition of cetyltrimethylammonium bromide (CTAB) with the concentration of 1 CEC to the MMT suspension. Step three—dissolving 1 g of zinc chloride in 20 mL of distilled water and adjustment of solution pH to 12.5 using sodium hydroxide solution. Step four—mixing the prepared suspensions in steps two and three for 6 h Step five—separation of suspended

ZnO/MMT particles from the aqueous solution by centrifugal separator. Step six—washing with distilled water and centrifuging to remove any non-adhesive impurities from ZnO/MMT particles. Step seven—drying ZnO/MMT particles at 90 °C for 3 h to remove moisture. ZnO nanoparticles were synthesized using the methods described in steps three to five of ZnO/MMT preparation method.

2.3. ZnO/MMT nanocomposite characterization

The ZnO nanoparticles, MMT particles and ZnO/MMT nanocomposite were characterized using powder X-ray diffraction (XRD), scanning electron microscopy (SEM), Fourier transform infrared (FT–IR) and N_2 adsorption/desorption apparatuses. XRD was done by the PANalytical X'Pert PRO apparatus (Germany) with monochromatic Cu$K\alpha$ X-radiation (45 kV, 40 mA, 0.15406 nm). The surface morphology of the material was studied by SEM model Mira3 FEG-SEM (Tescan, Czech) and HR-TEM model JEOL JEM-2100F (Japan) operated at 200 kV. FT-IR spectra were recorded by Tensor 27, Bruker spectrometer (Germany). Textural properties of the ZnO and ZnO/MMT samples were determined from N_2 adsorption/desorption isotherms at 77 K on a Gemini 2385 nitrogen adsorption apparatus (Micromeritics Instruments, USA) and their pore structure analyzed using Brunauer–Emmett–Teller (BET), and Barrett–Joyner–Halenda (BJH) equations. The generated reaction intermediates during the photocatalytic ozonation process at optimum conditions were identified using a gas chromatograph (6890, Agilent Technologies, CA) coupled with a mass spectrometer (5973, Agilent Technologies, Canada).

2.4. Metronidazole removal experiment

All experiments were conducted in a batch cylindrical quartz tube with total capacity of 900 mL. In a typical procedure, the degradation reactions were initiated by continuously UV-A illumination (nominal power of 8 W) and ozone bubbling into the quartz tube contains ZnO/MMT nanocomposite and MET solution with desired concentrations and pH. All the experiments were carried out at room temperature. To determine the variation of MET concentration during the photocatalytic ozonation process at pre-selected time intervals, samples were withdrawn from the tube and analyzed spectrophotometrically at 317 nm using a UV spectrophotometer (Varian Cary 100 UV–vis Spectrophotometer, Australia).

The removal efficiency (%) for each sample was equal to $(C_0 - C_t)/C_0$ where C_0 and C_t (mg/L) are the initial and the final concentrations of MET in the solution, respectively. In the case of photocatalytic degradation experiments, the similar process to photocatalytic ozonation was used except ozone bubbling into the quartz tube. Dissolved ozone concentration for different processes was determined by the procedure proposed by Bader and Hoigne [12].
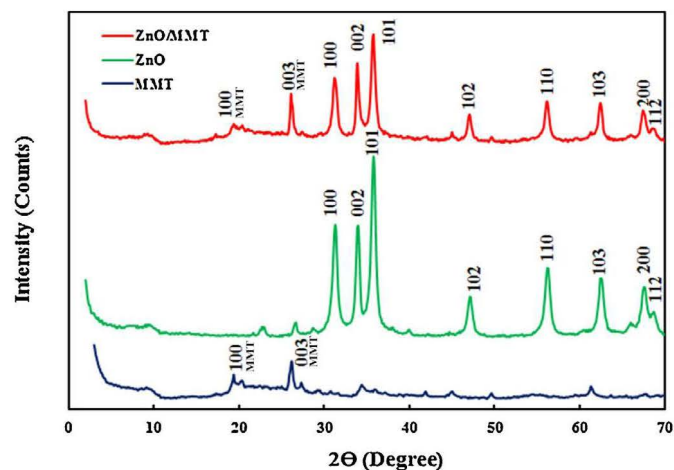
Fig. 1. XRD patterns of pure MMT, ZnO nanoparticles and ZnO/MMT nanocomposite.

2.5. Analysis of degradation products

GC–MS analysis was done to identify the intermediates of MET degradation through the photocatalytic ozonation process. 1 L of MET solution was treated for 10 min and the organic intermediates were extracted with 30 mL of diethyl ether three times. The obtained organic solution was held to evaporate the organic solvent and the remaining solid was dissolved in 100 μL of N,O-bis-(trimethylsilyl)acetamide under heating at 60 °C and stirring for 10 min. The obtained products were analyzed by GC–MS apparatus (Agilent 6890 gas chromatography and 5973 mass spectrometer, Palo Alto, Canada).

3. Results and discussion

3.1. Characterization of the nanocomposite

In order to investigate the effect of ZnO nanoparticles immobilization on theirs crystallographic structures, XRD patterns of pure MMT, ZnO nanoparticles and ZnO/MMT nanocomposite were taken as shown in Fig. 1. The peak at $2\theta = 26.1$ in XRD pattern of MMT and ZnO/MMT corresponds to MMT interlayer spacing [13]. Moreover, in the XRD pattern of ZnO and ZnO/MMT, the peaks at $2\theta = 31.37$, 34.03, 35.86, 47.16, 56.26, 62.54, 67.64 and 68.80 are corresponding to the 100, 002, 101, 102, 110, 103, 200 and 112 crystal plate of ZnO crystal, respectively [14]. The average crystal size of ZnO is 25 nm in pure ZnO and ZnO/MMT samples according to Scherrer equation. Comparison with ZnO nanoparticles, the peak locations of ZnO/MMT are the same except the peak at $2\theta=26.1$ which is attributed to MMT. Comparison of the ZnO and ZnO/MMT patterns clearly indicates that the ZnO nanoparticles in both pure and immobilized form have a same structure with all major peaks matching well with the standard pattern of bulk ZnO (JCPDS 36–1451) [14].

FT-IR studies of the pure MMT, ZnO and ZnO/MMT samples are carried out in the region 4000–400 cm^{-1} to find out the changes in the MMT and ZnO structures after immobilization. The characteristic bands of obtained FT-IR spectra as well as assigned functional groups are summarized in Table 2. Comparison of the obtained results consolidates the presence of both ZnO nanoparticles and MMT in the prepared nanocomposite samples.
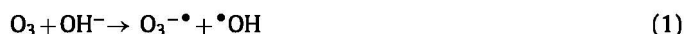
In order to support the results indicating the immobilization of fine ZnO particles on the surface of MMT particles, SEM and HR-TEM images of MMT and ZnO/MMT samples were taken (Figs. 2 and 3). The comparison of SEM and HR-TEM image of ZnO/MMT

sample with that of MMT sample approves the effective immobilization of ZnO particles. HR-TEM images display that the ZnO/MMT particles are within the nanoscale ($\leq$ 100 nm), supporting the results of SEM analysis which are shown in Fig. 3b.

N$_2$ adsorption/desorption isotherm of pure MMT, ZnO and ZnO/MMT samples were obtained (Fig. 4) to identify the porous structure of pure and immobilized ZnO nanoparticles. The N$_2$ adsorption/desorption on the MMT sample matches well the type II isotherm for mesoporous materials. Hysteresis loops of the N$_2$ adsorption/desorption on the MMT indicating the multi-layer physical adsorption on the surface of this adsorbent [19]. The ZnO and ZnO/MMT samples exhibit type IV nitrogen sorption isotherm according to the Brunauer–Deming –Deming–Teller (BDDT) classification with a capillary condensation step in the relative pressure (P/P_0) higher than 0.4. This approved a mesoporosity of both samples. The obtained results were analyzed using BET and BJH equation. Specific surface area and mesopore surface area of ZnO were 38.22 and 32.45 m^2/g, respectively while those of ZnO/MMT were enhanced to 70.54 and 84.97, respectively. The incorporation of ZnO and MMT caused to increase in available surface area for adsorption and photocatalytic ozonation of pollutant on the surface of ZnO nanoparticles.

3.2. Degradation of MET in different systems

Seven MET removal processes, namely adsorption, photolysis, photocatalysis, ozonation, photolytic ozonation, catalytic ozonation and, photocatalytic ozonation processes were conducted to evaluate the removal efficiency. Fig. 5 illustrates removal efficiency of all investigated processes under the same operational conditions. As shown in Fig. 5, when MET solution was subjected to ZnO/MMT, removal efficiency of 7.5% was achieved after 30 min which indicates low ability of ZnO/MMT as MET adsorbent. The MET hardly degraded when UV-A irradiation was applied to the polluted solution alone as photolysis process. It is due to the fact that very small amount of $^\bullet$OH is formed in the presence of UV-A radiation alone and/or the MET is relatively resistant to UV-A light [20]. In the presence of ZnO/MMT and UV-A light, more than two times increase in removal efficiency occurs which approved the effective role of the used catalyst in the photodegradation process. The ozonation removed 77.2% of the initial MET, which was due to the direct oxidation and/or generation of hydroxyl radicals (Eqs. (1–3)) [21].

$$O_3 + OH^- \rightarrow O_3^{-\bullet} + {}^\bullet OH \tag{1}$$

$$O_3^{-\bullet} \rightarrow O^{-\bullet} + O_2 \tag{2}$$

$$O^{-\bullet} + H^+ \rightarrow {}_\bullet OH \tag{3}$$

Simultaneously using UV-A irradiation and ozone in photolytic ozonation process improved the removal efficiency (81.28%) as a result of the fact that reactive radicals could be generated via following reactions (Eqs. (4 and 5)) [21].

$$O_3 + H_2O + h\nu \rightarrow O_2 + H_2O_2 \tag{4}$$

$$H_2O_2 + h\nu \rightarrow 2^\bullet OH \tag{5}$$

Combination of ZnO/MMT nanocomposite and the ozone had a beneficial effect on enhancing the MET removal efficiency. This enhancement in the MET removal efficiency can be attributed to simultaneous adsorption of ozone and pollutants molecules to efficient degradation reactions. A synergy value of 97% removal efficiency was obtained for the MET photocatalytic ozonation indicating that the combination of photolysis, photocatalysis, ozonation,

Table 2
FT-IR spectra information for the pure MMT, ZnO nanoparticles and ZnO/MMT nanocomposite.

Spectrum	Wave number (cm^{-1})	Group name	Reference
MMT and ZnO/MMT	793	Al–O stretching vibration	[15]
	1050	Si–O–Si in-plane stretching vibration	[16]
	2854	C–H symmetric vibration	[17]
	2928	C–H asymmetric vibration	[17]
	3437	O–H stretching vibration	[18]
	3622	Al–OH or Si–OH stretching vibration	[16]
ZnO and ZnO/MMT	424	Zn–O stretching vibration	[16]
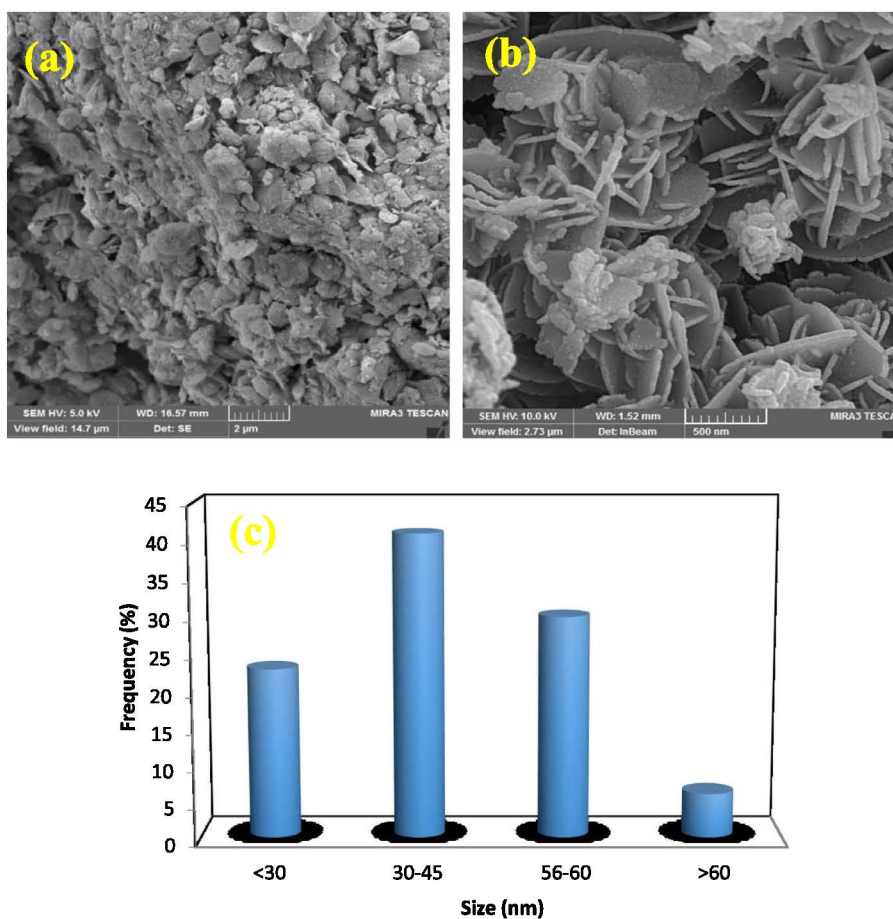
Fig. 2. SEM images of (a) raw MMT and (b) ZnO/MMT nanocomposite and (c) size distribution of ZnO/MMT nanocomposite.
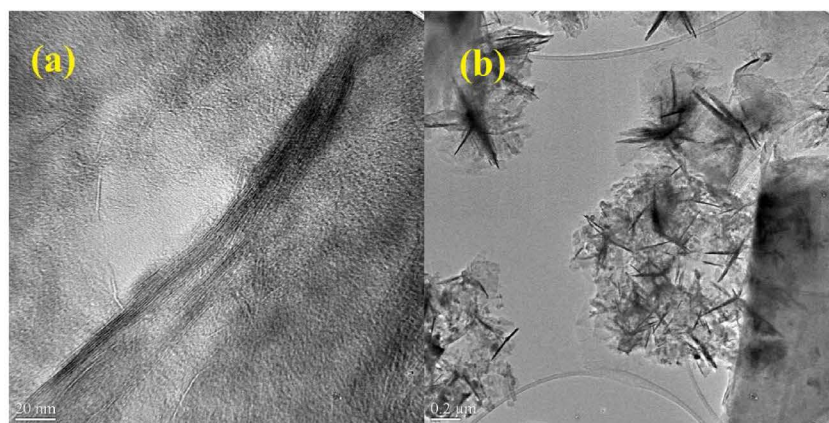

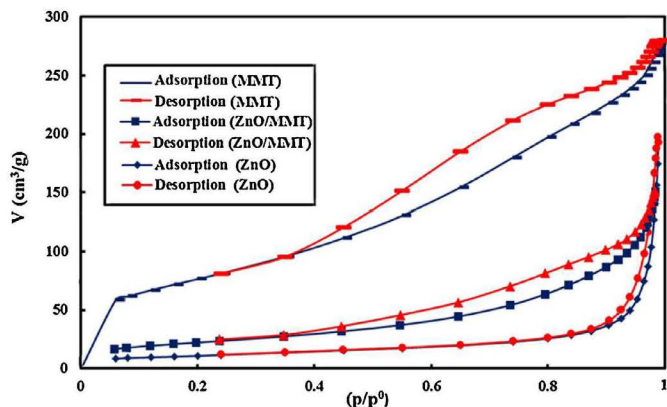**Fig. 3.** HRTEM images of (a) raw MMT and (b) ZnO/MMT nanocomposite.

Fig. 4. N_2 adsorption/desorption isotherms curves for pure MMT, ZnO nanoparticles and ZnO/MMT nanocomposite.
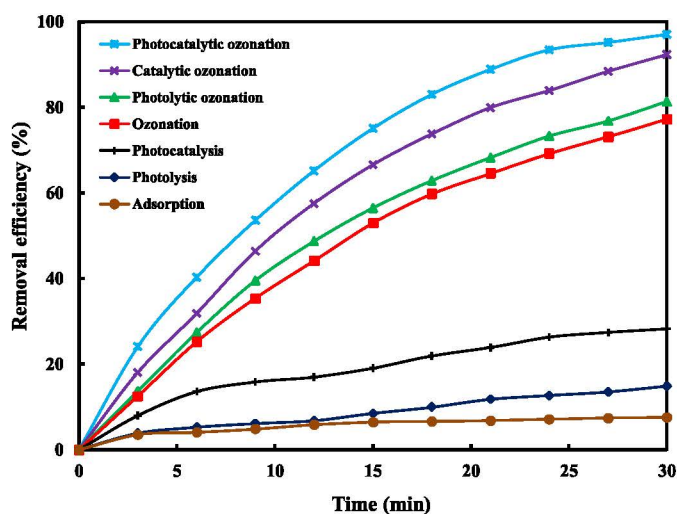

Fig. 5. MET removal efficiency (%) during various experiments. Experimental conditions: $[MET]_0$: 40 mg/L, ozone gas flow rate: 4 L/h, $[ZnO/MMT]_0 = 40$ mg/L, and pH = 6.

Fig. 6. Time evolution of dissolved ozone concentration during different oxidation processes. Experimental conditions: $[MET]_0$: 40 mg/L, ozone gas flow rate: 4 L/h, $[ZnO/MMT]_0 = 40$ mg/L, and pH = 6.

tion clearly revealed the higher number of reactions of ozone consumption such as the following reactions [14].

$$ZnO\text{-}e^- + O_3 \rightarrow ZnO^-O_3^{-\bullet} \tag{6}$$

$$ZnO\text{-}O_3^{-\bullet} + H^+ \rightarrow ZnO + HO_3^\bullet \tag{7}$$

$$HO_3^\bullet + {}^\bullet OH + O_2 \tag{8}$$

Accordingly, these results approve the contribution of synergistic effect between photocatalysis and ozonation processes for the improved removal of MET in the photocatalytic ozonation process. With the addition of MET, in both catalytic ozonation and photocatalytic ozonation processes, the decrease in dissolved ozone concentration shows the MET degradation by using radicals.

3.3. Effect of parameters on degradation efficiency

3.3.1. Effect of ozone flow rate

It is found that ozone flow rate is very important factor that controls ozonation process. To determine the optimum ozone flow rate, a number of MET degradation experiments have been made at pH of 6 and initial MET concentration of 40 mg/L while ozone flow rate was 1–6 L/h. Time profiles of MET degradation in the presence of different of inlet ozone flow rate is shown in Fig. 7. The ozone flow rates have a positive effect on the MET degradation through ozonation process. Enhancing the applied flow rate of ozone stream leads to increase in ozone mass transfer rate from gas to liquid phases. This causes an increased ozone and accordingly reactive radical concentration in the liquid phase which lead to increase in MET degradation efficiency. Similar phenomena have also been reported by M. Fathinia and Al. Khataee for photocatalytic ozonation of phenazopyridine using TiO_2 nanoparticles coated on ceramic plates [22].

3.3.2. Effect of pH

To determine the optimum pH of photocatalytic ozonation process, pH of MET degradation suspension was changed between 2 and 10 while initial MET concentration was 40 mg/L, ozone gas flow rate was 4 L/h and ZnO/MMT dosage was 40 mg/L as illustrated in Fig. 8. The removal efficiency increases with increasing pH up to 10. It can be explained based on the MET speciation diagrams and ZnO/MMT surface charge. At pH less than 4, MET is present as protonated specie while at pH higher than 12 it is present as anionic specie [23]. However, it is present as neutral

photolytic ozonation and catalytic ozonation processes favors pollutant degradation which may be attributed to the additional generation of hydroxyl radicals through mentioned reactions.

On the other hand, the dissolved ozone concentrations in different oxidation processes depending on the time were determined and evaluated. Fig. 6 illustrates the dissolved ozone concentration along with time for the ozonation, catalytic ozonation and photocatalytic ozonation processes in the presence and absence of MET. As can be seen from Fig. 6, the highest dissolved ozone concentration measured in the ozonation system. Its concentration increased up to 20 min, and then remained constant upon reaching an equilibrium accumulation of ozone in the aqueous phase. The reason for this phenomena is probably low ozone solubility and slow ozone gas–liquid reactions which cause to the hydroxyl radical generation [14]. The value of dissolved ozone amount dropped with the addition of MET, implying MET degradation through ozone molecules by direct pathway and/or hydroxyl radicals produced by indirect pathway. The dissolved ozone concentration in catalytic ozonation was considerably reduced in accordance with Fig. 5. This result can be attributed to that total effect of the adsorption of ozone molecules via the weak hydrogen bonds to the ZnO/MMT surface (absence of MET), and the improvement role of catalyst in MET degradation (presence of MET) by providing the increase in the number of reactive oxygen species (ROS) generated. The lowest dissolved ozone concentration for photocatalytic ozona-
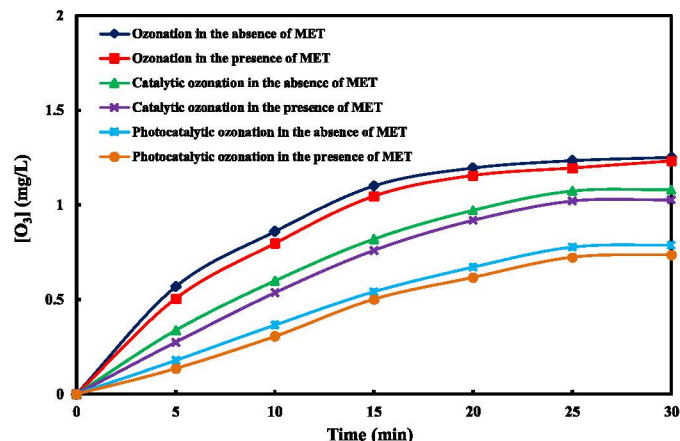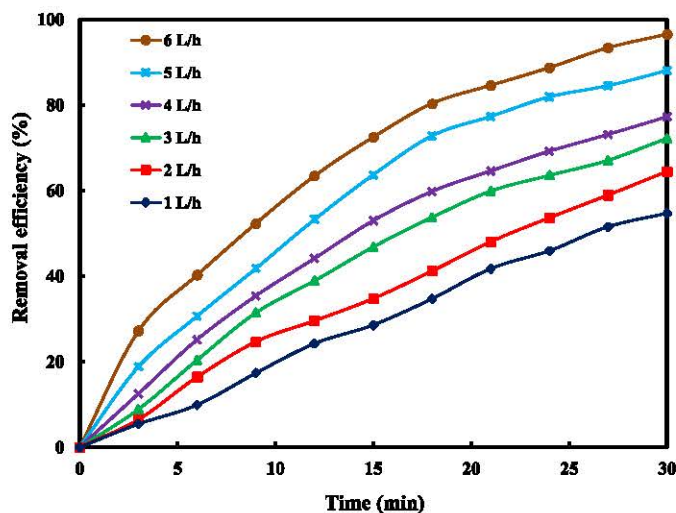
Fig. 7. Effect of inlet ozone flow rate on the ozonation of MET. Experimental conditions: $[MET]_0$: 40 mg/L, and pH = 6.
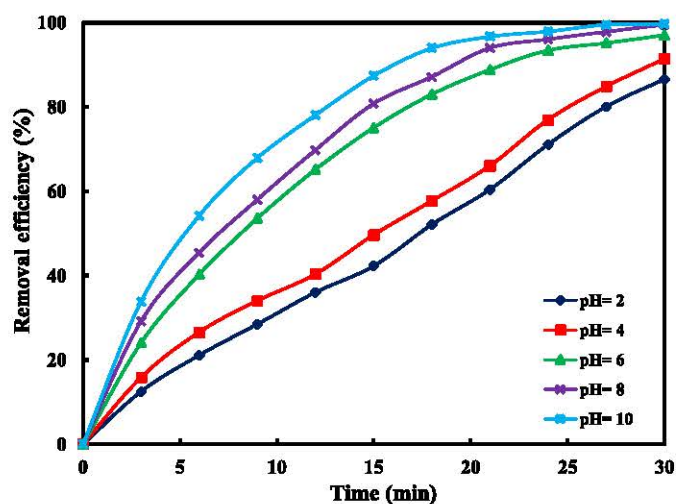

Fig. 8. Effect of initial pH value on the photocatalytic ozonation of MET. Experimental conditions: $[MET]_0$: 40 mg/L, ozone gas flow rate: 4 L/h, and $[ZnO/MMT]_0$ = 40 mg/L.

Fig. 9. Effect of the ZnO/MMT nanocomposite dosage on the photocatalytic ozonation of MET. Experimental conditions: $[MET]_0$ = 40 mg/L, ozone gas flow rate: 4 L/h, and pH = 6.

Fig. 10. Effect of initial MET concentration on the photocatalytic ozonation of MET. Experimental conditions: $[ZnO/MMT]_0$ = 40 mg/L, ozone gas flow rate: 4 L/h, and pH = 6.

specie at pH between 4 and 12 [23]. On the other hand, the pH of zero point charge (pH_{ZPC}) of ZnO/MMT nanoparticles was determined using the salt addition method [24]. pH_{ZPC} of the ZnO/MMT nanocomposite was approximately 8.4. Thus, in suspensions with pH of lower than 8.4 where pH is below ZnO/MMT nanoparticles pH_{ZPC}, it exhibits a positive net charge on its surface. Thus at pHs of 2 and 4, tendency of protonated MET to come closer to positively charged ZnO/MMT surface to react with developed reactive radicals was low. However, under natural and alkaline conditions the MET which mainly in the neutral form can come closer to the ZnO/MMT nanoparticles surface, resulting in its degradation via developed reactive species on the catalyst surface. Furthermore, the ozone is stable at acidic, while with increasing pH, efficiency of its decomposition to hydroxyl radicals was increased according to the Eq. (1). Accordingly, increase in suspension pH up to 10 leads to increase in MET removal efficiency.

3.3.3. Effect of ZnO/MMT nanocomposite dosage

The effect of ZnO/MMT nanocomposite dosage on the removal efficiency of MET was investigated while initial MET concentration was 40 mg/L and ozone gas flow rate was 4 L/h at pH of 6. The results are shown in Fig. 9. It was found that ZnO/MMT
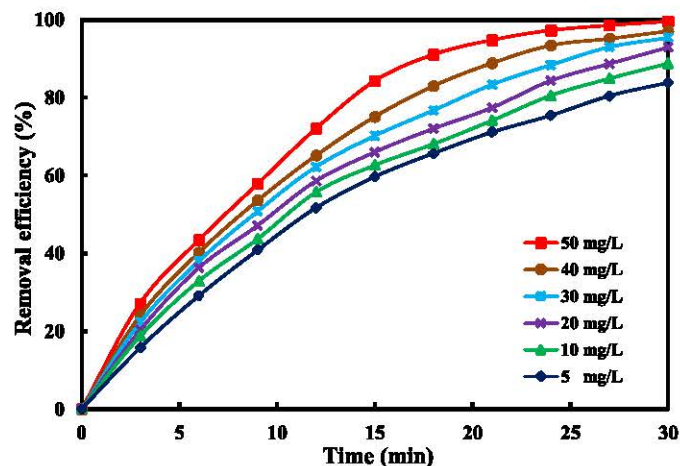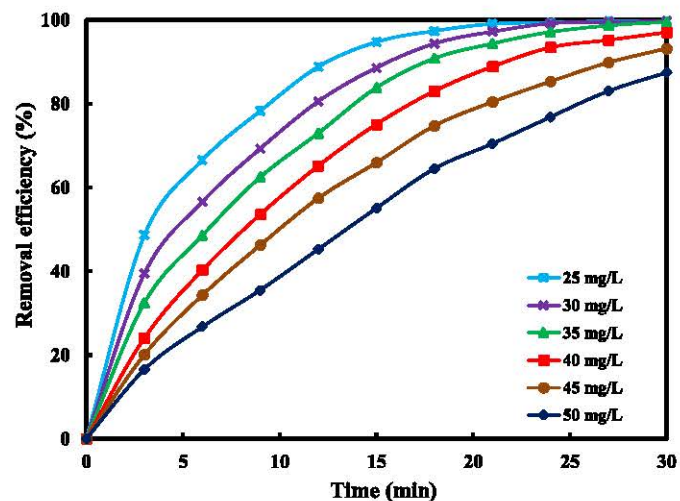
nanocomposite dosage of 50 mg/L gave the best results in the range of 5–50 mg/L. MET removal efficiency was enhanced with ZnO/MMT nanocomposite concentration at all investigated reaction times. It is reasonable because as ZnO/MMT nanocomposite dosage increases, the number of reactive catalytic sites increases.

3.3.4. Effect of initial metronidazole concentration

The efficiency of degradation through advanced oxidation process is a function of the initial pollutant concentration. Fig. 10 shows that the ability of the photocatalytic ozonation process in the MET removal with a ZnO/MMT loading of 40 mg/L and ozone gas flow rate of 4 L/h decreased with the increasing initial concentration of pollutant from 25 to 50 mg/L. There are two most probable reasons for the experimental observation. Firstly, concentrated pollutant solution may prohibit ZnO/MMT particles from absorbing eradiated UV-A waves. Furthermore, in the presence of high initial pollutant concentration, more degradation should be taken place to achieve the same value of degradation efficiency.

3.3.5. Stability and reusability of the ZnO/MMT nanocomposite catalyst

Considering that the stability of a typical catalyst is principal factor in its practical application, stability of the ZnO/MMT
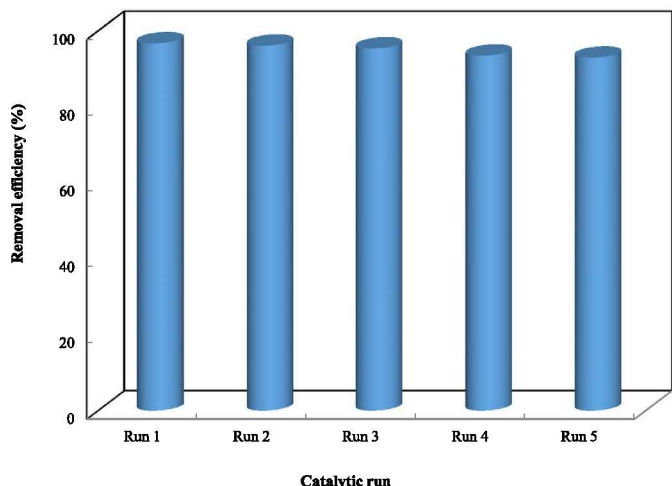
Fig. 11. Reusability of the ZnO/MMT nanocomposite in photocatalytic ozonation of MET. Experimental conditions: [MET]$_0$: 40 mg/L, ozone gas flow rate: 4 L/h, [ZnO/MMT]$_0$ = 40 mg/L, and pH = 6.
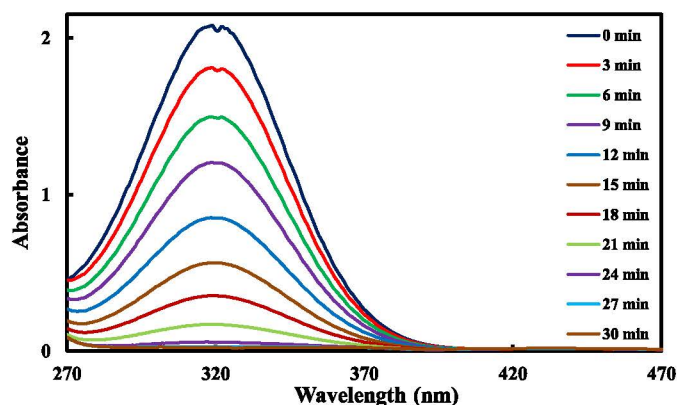

Fig. 12. The changes in the absorption spectra of MET during 30 min of photocatalytic ozonation process. Experimental conditions: [MET]$_0$: 40 mg/L, ozone gas flow rate: 4 L/h, [ZnO/MMT]$_0$ = 40 mg/L, and pH = 6.

nanocomposite catalyst in five subsequent photocatalytic ozonation of MET cycles under identical conditions was investigated. Each cycle consists of photocatalytic ozonation and then recovering by centrifugation, washing and drying of applied ZnO/MMT catalyst to use in next experiment. Obtained results (Fig. 11) indicate that about 97% removal efficiency takes place at 60 min in the first run. Fifth run gave 93% removal efficiency. This shows a negligible decrease in the removal efficiency even after using one ZnO/MMT sample in five successive photocatalytic ozonation run. Obtained result approves good mechanical and chemical stability of the applied ZnO/MMT catalyst to be used as a promising catalyst for the degradation of organic pollutants.

3.3.6. Spectral changes of MET during photocatalytic ozonation

Fig. 12 illustrates the changes in the absorption spectra of the MET solution during photocatalytic ozonation process in the presence of initial 40 mg/L MET at 40 mg/L ZnO/MMT at pH of 6 under ozone gas flow rate of 4 L/h and UV-A irradiation. The absorption peak of MET is located at 317 nm. The decrease in the absorption peak intensity and finally its disappearance with increase of the reaction time actually indicates the MET degradation during photocatalytic ozonation process.

3.3.7. Effect of organic and inorganic radical scavengers

To specify the most effective MET degradation mechanisms through the photocatalytic ozonation process, several degradation
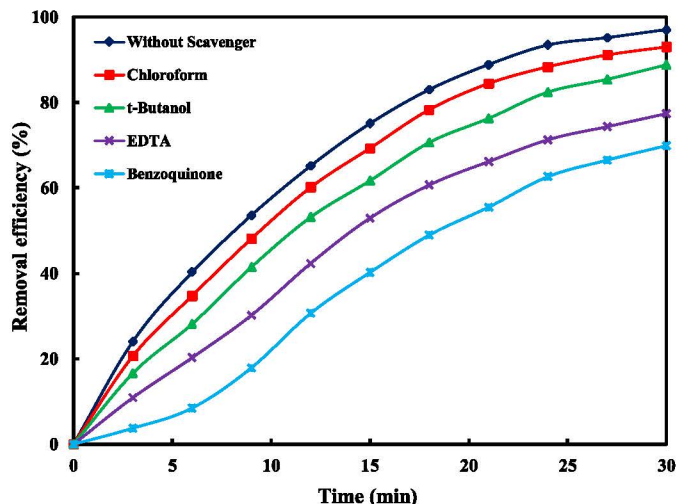

Fig. 13. Effect of the organic radical scavengers on the photocatalytic ozonation removal of MET. Experimental conditions: [MET]$_0$: 40 mg/L, ozone gas flow rate: 4 L/h, [ZnO/MMT]$_0$ = 40 mg/L, [Radical scavenger] = 40 mg/L, and pH = 6.

Fig. 14. Effect of the inorganic radical scavengers on the photocatalytic ozonation removal of MET. Experimental conditions: [MET]$_0$: 40 mg/L, ozone gas flow rate: 4 L/h, [ZnO/MMT]$_0$ = 40 mg/L, [Radical scavenger] = 40 mg/L, and pH = 6.
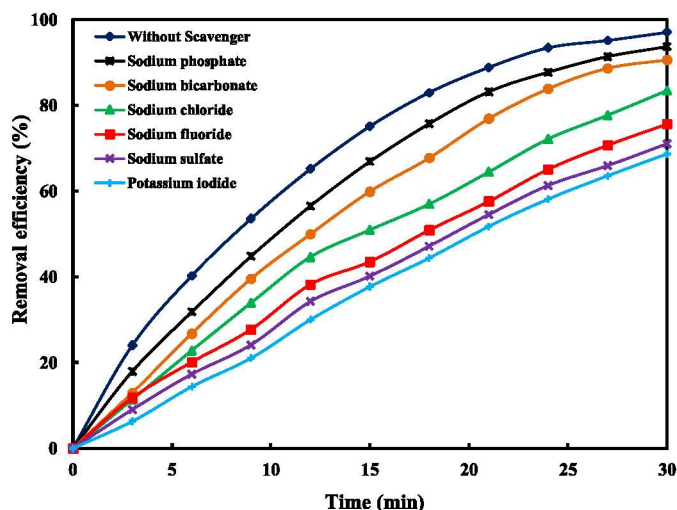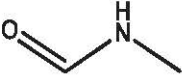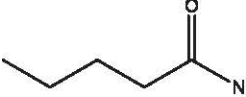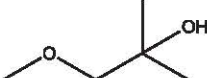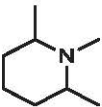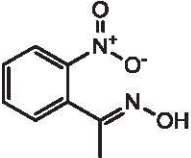
tests were run in the presence of various organic and inorganic radical quenchers. Fig. 13 shows that the photocatalytic ozonation removal of MET was inhibited by the addition of benzoquinone, chloroform, t-butanol and EDTA as organic radical quenchers. In the presence of these quenchers, the decreased MET removal efficiency with the order of significance following benzoquinone > EDTA > t-butanol > chloroform. Benzoquinone and chloroform as effective O$_2^{-\bullet}$ quencher exhibited higher and lower effect on photocatalytic ozonation removal of MET, respectively [25,26]. On the contrary, EDTA and t-butanol as hydroxyl radical scavengers exerted moderated decreasing effect on the MET removal efficiency [27,28]. These results demonstrates that both $^\bullet$OH and O$_2^{-\bullet}$ are produced and participated in degradation of MET through photocatalytic ozonation process and presence of both kind of scavenger reduce the process efficiency.

Furthermore, effect of common inorganic anions in natural water and wastewater including sulfate, chloride, fluoride, bicarbonate, phosphate and iodide on performance of photocatalytic ozonation process was conducted (Fig. 14). Among investigated inorganic radical scavenger, the iodide and sulfate anions show higher decreasing effect on the process. Iodide effects on MET degradation

Table 3
Identified by-products during the photocatalytic ozonation of 40 mg/L MET.

No	Compound name	Chemical structure	Retention time (min)	Main fragments
1	N-Methyl-formamide		2.629	59.00 (100.00%); 75.00 (3.98%); 60.00 (2.73%); 86.10 (2.33%); 91.00 (1.28%)
2	2-Hexanone		2.784	59.00 (100.00%); 75.00 (7.35%); 86.10 (3.88%); 60.00 (2.70%); 146.90 (1.34%)
3	1-Methoxy-2-methyl-2-propanol		3.439	59.00 (100.00%); 75.00 (38.22%); 62.90 (24.39%); 207.00 (20.08%); 86.10 (17.22%)
4	Piperidine, 1,2,6-trimethyl		3.572	59.00 (100.00%); 112.00 (75.88%); 75.00 (54.78%); 77.00 (43.47%); 113.90 (24.66%)
5	O-Nitroacetophenone oxime		31.391	148.90 (100.00%); 207.00 (75.97%); 55.00 (36.21%); 166.90 (33.53%); 57.10 (28.36%)

process through following most probable reasons including fast reaction with ozone to form the hypoiodite ion (Eq. 9) and scavenging hydroxyl radicals produced through photocatalytic ozonation process (Eqs. 10 and 11). [29,30]

$$I^- + O_3 \rightarrow I_2 + IO^- + O_2 \tag{9}$$

$$I^- + {}^\bullet OH \rightarrow I^\bullet + OH \tag{10}$$

$$I^\bullet + I^- \rightarrow I_2^{\bullet -} \tag{11}$$

In the presence of 40 mg/L sodium sulfate, more than 26% decrease in the MET removal efficiency was observed after 30 min reaction time. This can be attributed to considerable h^+ and hydroxyl radical quenching ability of this anion which cause to production of less reactive $SO_4^{\bullet -}$ radicals [31].

Presence of 40 mg/L NaF, led to more than 21% decrease in MET removal efficiency. The most probable reason for the photocatalytic ozonation efficiency decrease is ZnO/MMT surface sites blocking by F^- ions due to strong adsorption ability of the fluoride ions on the surface of the nanocomposite and accordingly inhibition of ozone and MET adsorption and decomposition on the surface of ZnO/MMT [32]. Furthermore, fluoride ions exhibit scavenging effect on the photo-generated h^+ of ZnO/MMT photocatalyst [33].

Bicarbonate ions can act as hydroxyl radical scavenger forming less reactive carbonate radicals as well as exhibit scavenging effect on the photo-generated h^+, thus decrease the MET removal efficiency from 97% to 90.6% [34].

Obtained results indicate that effect of phosphate anion was lower than that of other anions. Phosphate anions not only are considered as weak scavengers of reactive radicals but also may quench photo-generated e^- of ZnO/MMT photocatalyst and accordingly enhance contribution of photo-generated h^+ in reactive radicals production process [35,36].

3.3.8. Analysis of degradation intermediates of MET during photocatalytic ozonation

To identify the degradation intermediates of MET during photocatalytic ozonation process, the generated by products after 15 min are analyzed three times by GC–MS [37]. The obtained general peaks for three analyses was selected and evaluated.

The formed by-products were assessed by comparing the recorded spectra in the mass spectra library. The obtained results were given in Table 3.

4. Conclusions

Stabilizing of ZnO nanoparticles and its application in photocatalytic ozonation is one of the effective ways to improve the ZnO photocatalytic efficiency. The results showed that photocatalytic ozonation activity depends on the ozone flow rate, ZnO/MMT dosage, metronidazole initial concentration and pH. The determined dissolved ozone concentration confirmed synergetic effects of the photocatalytic ozonation process on MET degradation. ZnO/MMT nanocomposite has good mechanical and chemical stability. Furthermore, the organic and inorganic free radical scavengers have a decreasing effect on the photocatalytic ozonation of metronidazole.

Acknowledgments

References

[1] Daghrir R, Drogui P, El Khakani MA. Photoelectrocatalytic oxidation of chlortetracycline using Ti/TiO₂ photo-anode with simultaneous H₂O₂ production. Electrochim Acta 2013;87:18–31.
[2] Le-Minh N, Khan SJ, Drewes JE, Stuetz RM. Fate of antibiotics during municipal water recycling treatment processes. Water Res 2010;44:4295–323.

[3] Sheydaei M, Aber S, Khataee A. Degradation of amoxicillin in aqueous solution using nanolepidocrocite chips/H_2O_2/UV: optimization and kinetics studies. J Ind Eng Chem 2013;20:1772–8.

[4] Khataee AR, Fathinia M, Joo SW. Simultaneous monitoring of photocatalysis of three pharmaceuticals by immobilized TiO_2 nanoparticles: Chemometric assessment, intermediates identification and ecotoxicological evaluation. Spectrochim Acta, Part A 2013;112:33–45.

[5] Ayoubi-Feiz B, Aber S, Sheydaei M. Effect of oxidants on photoelectrocatalytic decolourization using α-Fe_2O_3/TiO_2/activated charcoal plate nanocomposite under visible light. RSC Adv 2015;5:19368–78.

[6] Kıranşan M, Khataee A, Karaca S, Sheydaei M. Artificial neural network modeling of photocatalytic removal of a disperse dye using synthesized of ZnO nanoparticles on montmorillonite. Spectrochim Acta, Part A 2015;140:465–73.

[7] Ayoubi-Feiz B, Aber S, Khataee A, Alipour E. Electrosorption and photocatalytic one-stage combined process using a new type of nanosized TiO_2/activated charcoal plate electrode. Environ Sci Pollut Res 2014;21:8555–64.

[8] Yin J, Liao G, Zhu D, Lu P, Li L. Photocatalytic ozonation of oxalic acid by g-C3N4/graphene composites under simulated solar irradiation. J Photochem Photobiol, A 2016;315:138–44.

[9] Fathinia M, Khataee A, Aber S, Naseri A. Development of kinetic models for photocatalytic ozonation of phenazopyridine on $TiO2$ nanoparticles thin film in a mixed semi-batch photoreactor. Appl Catal B 2016;184:270–84.

[10] Moreira NFF, Sousa JM, Macedo G, Ribeiro AR, Barreiros L, Pedrosa M,, et al. Photocatalytic ozonation of urban wastewater and surface water using immobilized $TiO2$ with LEDs: micropollutants, antibiotic resistance genes and estrogenic activity. Water Res 2016;94:10–22.

[11] Moreira NFF, Orge CA, Ribeiro AR, Faria JL, Nunes OC, Pereira MFR, et al. Fast mineralization and detoxification of amoxicillin and diclofenac by photocatalytic ozonation and application to an urban wastewater. Water Res 2015;87:87–96.

[12] Bader H, Hoigné J. Determination of ozone in water by the indigo method. Water Res 1981;15:449–56.

[13] Rasouli F, Aber S, Salari D, Khataee AR. Optimized removal of Reactive Navy Blue SP-BR by organo-montmorillonite based adsorbents through central composite design. Appl Clay Sci 2014;87:228–34.

[14] Khataee A, Darvishi Cheshmeh Soltani R, Hanifehpour Y, Safarpour M, Gholipour Ranjbar H, Joo SW. Synthesis and characterization of dysprosium-doped ZnO nanoparticles for photocatalysis of a textile dye under visible light irradiation. Ind Eng Chem Res 2014;53:1924–32.

[15] Kıranşan M, Khataee A, Karaca S, Sheydaei M. Synthesis of zinc oxide nanoparticles on montmorillonite for photocatalytic degradation of Basic Yellow 28: Effect of parameters and neural network modeling. Curr Nanosci 2015;11:343–53.

[16] Shirzad-Siboni M, Farrokhi M, Darvishi Cheshmeh Soltani R, Khataee A, Tajassosi S. Photocatalytic reduction of hexavalent chromium over ZnO nanorods immobilized on kaolin. Ind Eng Chem Res 2014;53:1079–87.

[17] Acisli O, Khataee A, Karaca S, Sheydaei M. Modification of nanosized natural montmorillonite for ultrasound-enhanced adsorption of Acid Red 17. Ultrason Sonochem 2016;31:116–21.

[18] Aber S, Khataee A, Sheydaei M. Optimization of activated carbon fiber preparation from Kenaf using K_2HPO_4 as chemical activator for adsorption of phenolic compounds. Bioresour Technol 2009;100:6586–91.

[19] Hassani A, Alidokht L, Khataee AR, Karaca S. Optimization of comparative removal of two structurally different basic dyes using coal as a low-cost and available adsorbent. J Taiwan Inst Chem Eng 2014;45:1597–607.

[20] Wang H, Zhang G, Gao Y. Photocatalytic degradation of metronidazole in aqueous solution by niobate K6Nb10.8O30. Wuhan Univ J Nat Sci 2010;15:345–9.

[21] Wu C.H., Ng H.Y. Degradation of C.I. Reactive Red 2 (RR2) using ozone-based systems: comparisons of decolorization efficiency and power consumption. J Hazard Mater 2008; 152: 120–7.

[22] Fathinia M, Khataee A. Photocatalytic ozonation of phenazopyridine using TiO_2 nanoparticles coated on ceramic plates: mechanistic studies, degradation intermediates and ecotoxicological assessments. Appl Catal, A 2015;491:136–54.

[23] Bellobono IR, Morelli R, Chiodaroli CM. Photocatalysis and promoted photocatalysis during photocrosslinking of multifunctional acrylates in composite membranes immobilizing titanium dioxide. J Photochem Photobiol, A 1997;105:89–94.

[24] Mustafa S, Dilara B, Nargis K, Naeem A, Shahida P. Surface properties of the mixed oxides of iron and silica. Colloids Surf, A 2002;205:273–82.

[25] Li N, Lu X, Zhang S. A novel reuse method for waste printed circuit boards as catalyst for wastewater bearing pyridine degradation. Chem Eng J 2014;257:253–61.

[26] Sun S-P, Lemley AT. p-Nitrophenol degradation by a heterogeneous Fenton-like reaction on nano-magnetite: process optimization, kinetics, and degradation pathways. J Mol Catal A: Chem 2011;349:71–9.

[27] Pignatello JJ, Oliveros E, MacKay A. Advanced oxidation processes for organic contaminant destruction based on the Fenton reaction and related chemistry. Crit Rev Environ Sci Technol 2006;36:1–84.

[28] Zeng X, Hanna K, Lemley AT. Cathodic Fenton degradation of 4,6-dinitro-o-cresol with nano-magnetite. J Mol Catal A: Chem 2011;339:1–7.

[29] Al-Bastaki NM. Treatment of synthetic industrial wastewater with UV/TiO_2 and RO using benzene as a model hydrocarbon. Desalination 2003;156:193–7.

[30] Xu L, Wang J. A heterogeneous Fenton-like system with nanoparticulate zero-valent iron for removal of 4-chloro-3-methyl phenol. J Hazard Mater 2011;186:256–64.

[31] Zhang W, An T, Cui M, Sheng G, Fu J. Effects of anions on the photocatalytic and photoelectrocatalytic degradation of reactive dye in a packed-bed reactor. J Chem Technol Biotechnol 2005;80:223–9.

[32] Ma Y, Zhang J, Tian B, Chen F, Bao S, Anpo M. Synthesis of visible light-driven Eu, N co-doped TiO_2 and the mechanism of the degradation of salicylic acid. Res Chem Intermed 2012;38:1947–60.

[33] Karaca M, Kiransan M, Karaca S, Khataee A, Karimi A. Sonocatalytic removal of naproxen by synthesized zinc oxide nanoparticles on montmorillonite. Ultrason Sonochem 2016;31:250–6.

[34] Hassani A, Khataee A, Karaca S. Photocatalytic degradation of ciprofloxacin by synthesized TiO_2 nanoparticles on montmorillonite: effect of operation parameters and artificial neural network modeling. J Mol Catal A: Chem 2015;409:149–61.

[35] Sowmya A, Meenakshi S. Photocatalytic reduction of nitrate over Ag–TiO_2 in the presence of oxalic acid. J Water Process Eng 2015;8:e23–30.

[36] Zhao W, Liu F, Yang Y, Tan M, Zhao D. Ozonation of Cationic Red X-GRL in aqueous solution: kinetics and modeling. J Hazard Mater 2011;187:526–33.

[37] Flox C, Ammar S, Arias C, Brillas E, Vargas-Zavala AV, Abdelhedi R. Electro-Fenton and photoelectro-Fenton degradation of indigo carmine in acidic aqueous medium. Appl Catal B 2006;67:93–104.